Journal Pre-proof

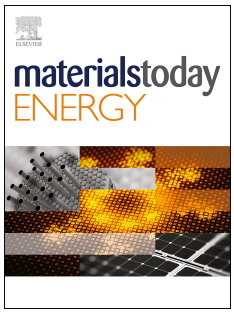

Controllable design of nanoworm-like nickel sulfides for efficient electrochemical water splitting in alkaline media

Zhijie Chen, Idris Ibrahim, Derek Hao, Xiaoqing Liu, Lan Wu, Wei Wei, Dawei Su, Bing-Jie Ni

PII: S2468-6069(20)30192-1

DOI: https://doi.org/10.1016/j.mtener.2020.100573

Reference: MTENER 100573

To appear in: *Materials Today Energy*

Received Date: 5 October 2020

Revised Date: 17 October 2020

Accepted Date: 20 October 2020

Please cite this article as: Z. Chen, I. Ibrahim, D. Hao, X. Liu, L. Wu, W. Wei, D. Su, B.-J. Ni, Controllable design of nanoworm-like nickel sulfides for efficient electrochemical water splitting in alkaline media, *Materials Today Energy*, https://doi.org/10.1016/j.mtener.2020.100573.

Graphical Abstract

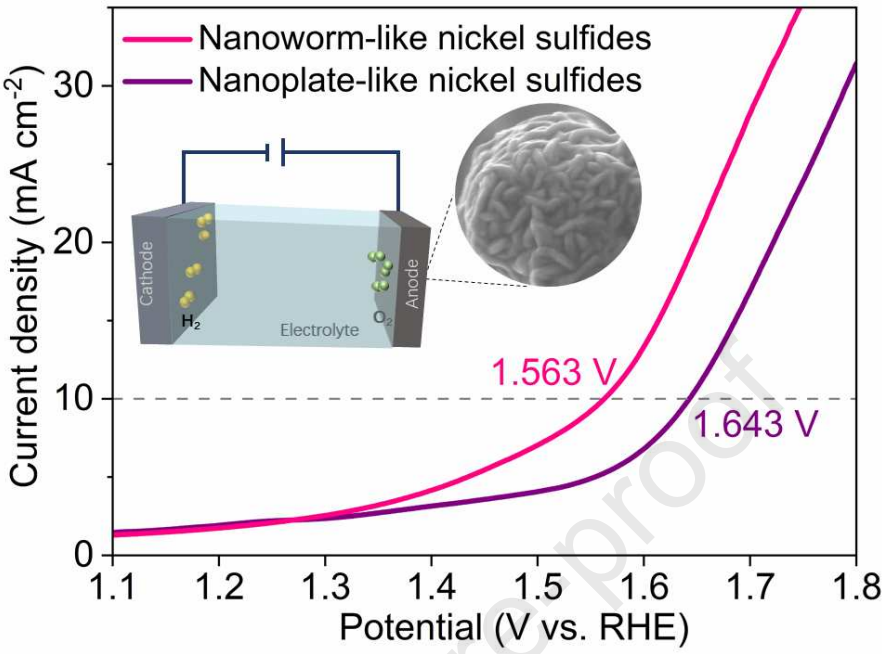

The nanoworm-like nickel sulfides developed by a one-step solvothermal strategy exhibit great performance for overall electrochemical water splitting, and a low voltage of 1.563 V is required to attain a current density of 10 mA cm^{-2} in a two-electrode electrolyzer.

Controllable design of nanoworm-like nickel sulfides for efficient electrochemical water splitting in alkaline media

Zhijie Chen,[a] Idris Ibrahim,[a] Derek Hao,[a] Xiaoqing Liu,[a] Lan Wu,[a] Wei Wei,[a] Dawei Su,[b,*] Bing-Jie Ni [a,*]

[a] *Centre for Technology in Water and Wastewater, School of Civil and Environmental Engineering, University of Technology Sydney, NSW 2007, Australia*

[b] *Center for Clean Energy Technology, School of Mathematical and Physical Science, Faculty of Science, University of Technology Sydney, NSW 2007, Australia*

*Corresponding Author:

Dawei Su E-mail: Dawei.Su@uts.edu.au

Bing-Jie Ni E-mail: bingjieni@gmail.com

Abstract

Developing cost-effective electrocatalysts for electrochemical water splitting (EWS) is appealing and challenging for sustainable water electrolysis. Currently, nickel sulfides are considered as promising candidates for EWS due to their low cost and high catalytic activity. However, the facile design of nickel sulfides with high catalytic performance is still highly demanded. In this study, we have developed a one-step solvothermal strategy to construct nickel sulfides as efficient water splitting catalysts. By taking advantage of the small size, abundant active sites, large electrochemical surface area, and good conductivity, the nanoworm-like nickel sulfides (NiS-NW/NF) exhibit better OER performance (a low overpotential of 279 mV to achieve 100 mA cm^{-2}, Tafel slope of 38.44 mV dce^{-1}) than the nanoplate-like analogues, as well as most of reported nickel sulfide-based electrocatalysts. Additionally, the NiS-NW/NF directly used as bifunctional electrodes for overall water splitting requires a low voltage of 1.563 V to attain a current density of 10 mA cm^{-2} with good long-term durability. This work provides a facile strategy for the design of efficient nickel sulfide-based electrocatalysts for energy conversion applications.

Keywords: Nickel sulfides; Morphology; Solvothermal synthesis; Oxygen evolution reaction; Overall water splitting

1. Introduction

Developing renewable energy technologies is an urgent issue to mitigate the impending energy crisis and the alarming environmental degradation. Electrochemical water splitting (EWS) is an efficient and clean way to produce hydrogen which is considered as a green energy carrier [1-3]. The EWS consists of two half reactions, the hydrogen evolution reaction (HER) at the cathode and the oxygen evolution reaction (OER) at the anode. Importantly, the efficiency of the EWS is highly dependent on the electrode materials, namely the catalysts. Noble metal (e.g., Pt, Ir, Pd, and Ru)-based catalysts have exhibited great performance for EWS, however the low reserve and high price of these materials significantly limit their commercial applications [4, 5]. As a result, it is imperative to develop low-cost and efficient electrocatalysts for EWS. To our delight, numerous earth-abundant materials have shown good catalytic performance for EWS [6], including transition metal-based materials [7-12] and metal-free materials [13-17]. Among these low-cost candidates, transition metal sulfides (TMSs) have attracted enormous attention as OER and HER catalysts due to the high intrinsic catalytic activity, good electrical conductivity, and structural stability.

Nanoscale TMSs have been widely studied for EWS, but their catalytic performance is still inferior to that of precious metal-based materials. To further improve the catalytic properties of TMSs, various efficient strategies have been employed, including chemical component regulation [1, 18], morphology control [19, 20], defect engineering [21, 22], and hybridization [23, 24], etc. Recent studies show that the morphology of nanocatalysts has a prominent effect on the catalytic performance of TMSs [25]. For example, Wu et al. [26] compared the catalytic performance of

three zinc cobalt mixed sulfide nanostructures with different morphologies, including nanosheets, nanoplates, and nanoneedles. The one-dimensional Zn-Co-S nanoneedles exhibited higher catalytic activities toward both HER and OER than the analogues. This is because the integrated Zn-Co-S nanoneedle/CFP nanostructure can provide enhanced electrochemical active area, facilitate ion transfer, and gas evolution. Similarly, You and co-workers investigated the correlation between morphology and HER activity of a series of CoS with different morphologies (hollow nanoprism, broken nanoprism, and nanoparticle) [27]. The CoS nanoparticle shows the largest specific surface area and electrochemically active surface area (ECSA), and these features result in the improved accessibility of electroactive sites, enhanced mass/charge transport and accelerated release of gas bubbles, rendering its highest HER performance and good durability. As a result, it is of great significance to tune the morphology of catalysts, and thus improve the surface active sites and the structural stability [28]. Although TMSs with different morphologies for EWS have been documented, the morphology-control synthesis of efficient NiS catalysts with facile methods is still challenging. Additionally, the relationship between the morphology-controlled catalysts and their catalytic properties needs further explorations.

Herein, we have developed a one-step solvothermal strategy to construct nickel sulfides as efficient water splitting catalysts. The morphology-dependent electrochemical performance is uncovered, and the nanoworm-like nickel sulfides (NiS-NW/NF) outperform the nanoplate-like counterpart. Benefiting from the small size, abundant active sites, large electrochemical surface area, and good conductivity, the NiS-NW/NF exhibits great OER performance (e.g., η_{100} = 279 mV, Tafel slope = 38.44 mV dce^{-1}) and good HER activity. When fabricated in a two-electrode cell,

only a voltage as low as 1.563 V was required to achieve a current density of 10 mA cm^{-2}.

2. Experimental section

2.1. Material synthesis

The NiS nanoworms (NW) were prepared using a solvothermal method. Briefly, Ni foam (NF) with a thickness of 1 mm was ultrasonically treated with 1M HCl, followed by acetone (≥99.5%, Sigma-Aldrich) and distilled water in order to remove the oxide layer. The growth solution was prepared by dissolving 2 mmol of thiourea (TU, ≥99.0%, Sigma-Aldrich) as sulfur source into 27 ml of isopropanol alcohol (IA, ≥99.5%, Sigma-Aldrich) under vigorous stirring at room temperature for 1 hour. After TU completed dissolved, 3 ml of glycerol (≥99.5%, Sigma-Aldrich) was added to the solution and continues stirring for another 30 min. Then, the mixed solution was transferred into a 50 ml autoclave followed by immersing NF (2×2 cm^2) and placed at a conventional oven at 180 ^oC for 3 hours. After the reaction completed it allowed to be cooled naturally. Finally, the as-obtained materials were washed with water and ethanol several times and dried at the vacuum oven for 4 h at 60 ^oC. Similarly, the NiS nanoplates (NP) were synthesized when 30 ml of IA was used, without the addition of glycerol. A series of NiS samples were prepared via changing the dosages of IA and glycerol, and the total amount of IA and glycerol was controlled at 30 ml.

2.2. Structural characterization

The structural morphology of the samples was analyzed using scanning electron microscopy (SEM, Zeiss Sigma 55VP). The crystal structure of the samples was determined by X-ray

diffraction (XRD) measurements on a Rigaku Smart Lab X-ray diffractometer operated at 40 kV using Cu Kα radiation. Transmission electron microscope (TEM) images were performed with a FEI Tecnai G2 F20 S-TWIN microscope with an acceleration voltage of 200 kV. The element composition of the material was analyzed by the X-ray photoelectron spectroscopy (XPS, Thermo K-Alpha$^+$, Thermo Fisher Scientific, USA) with the Al (Kα) radiation.

2.3. Electrochemical measurements

Electrochemical measurements were carried out with a CHI 760E electrochemical workstation. OER and HER activities were recorded in a three-electrode system with graphite rod as the counter electrode and Hg/HgO as the reference electrode in O_2-saturated and N_2-saturated 1.0 M KOH electrolytes, respectively. The as-prepared NF-supported samples were directly used as the working electrode. To prepare the IrO_2 electrode, 5 mg of IrO_2 powder (99.9%, Sigma-Aldrich) were dispersed in 1 mL of mixed solution (500 μL of water, 450 μL of ethanol, and 50 μL of 5 wt% Nafion solution). The 20 wt % Pt/C electrode was prepared with a similar process. After sonication for 30 min, a homogeneous ink was obtained. 100 μL of the ink was deposited onto a piece of acid treated NF. Linear sweep voltammetry (LSV) was performed at scan rate of 5 mV s^{-1} for both HER and OER. The polarization curves were calibrated with 90% iR compensation to eliminate the solution resistance. All potentials measured were converted to a reversible hydrogen electrode (RHE) using the following equation: $E_{vs\ RHE}=E_{vs\ Hg/HgO}$ + 0.098 V + 0.059 pH. Electrochemical impedance spectroscopy (EIS) was recorded at the open circuit potential over a frequency range of 10^{-1} to 10^5 Hz with an AC signal amplitude of 5 mV. The double-layer capacitances (C_{dl}) were calculated through cyclic voltammogram (CV) at different scan rates (i.e.,

40, 60, 80, 100, and 120 mV s^{-1}) in 1.0 M KOH. The Amperometric i-t curves were recorded to test the long-term stability of catalysts for both OER and HER, and for the overall water splitting.

3. Results and discussion

3.1. Material characterizations

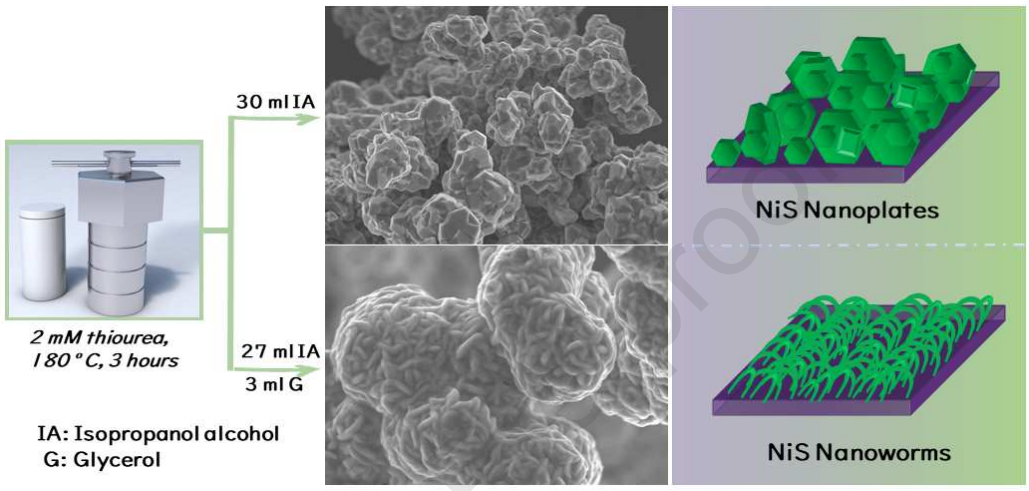

Fig. 1 Schematic of the formation of NiS-NW/NF and NiS-NP/NF.

Fig. 1 illustrates the synthesis procedure of the nickel sulfide samples, which only comprises a solvothermal sulfidization of direct growth of nickel sulfides on nickel foam. The appropriate addition of glycerol and IA as surfactants is the key for tuning the morphology of nickel sulfides. The nanoworm-like nickel sulfide sample (NiS-NW/NF) is obtained when a small amount (3 ml) of glycerol and 27 ml of IA are added as the solvent, while the nanoplate-like nickel sulfide sample (NiS-NP/NF) is formed with adding 30 ml of IA only. Compared with the NiS-NP/NF, the NiS-NW/NF possesses a smaller average size (~100 nm vs ~200 nm) and higher surface area (**Fig. 2a-b**). These features suggest that the NiS NWs may be more favorable for electrochemical reactions than the counterpart. In addition, the energy-dispersive spectroscopy (EDS) elemental mapping images of the NiS NWs (**Fig. 2c**) show the uniformly distribution of Ni and S.

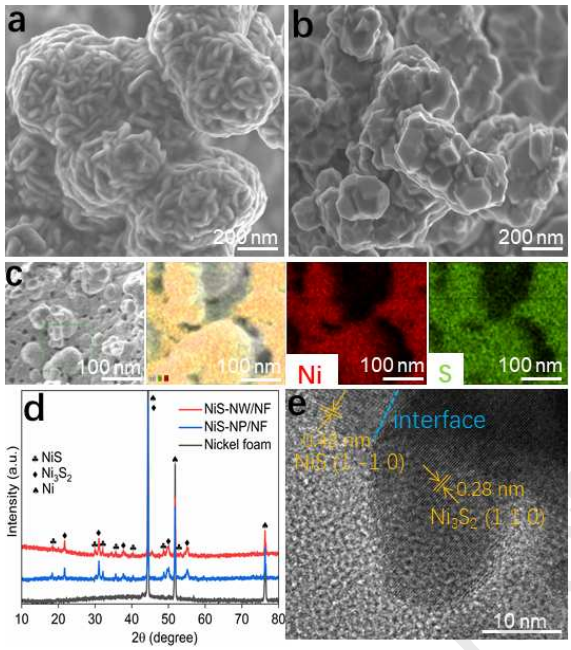

147

148 **Fig. 2** (a) SEM image of NiS-NW/NF, (b) SEM image of NiS-NP/NF, (c) SEM-EDS mapping of
149 NiS-NW/NF, (d) XRD patterns of NiS-NW/NF, NiS-NP/NF and bare Nickel foam, (e) HRTEM image
150 of NiS-NW/NF.

151 The crystal structures of the as-prepared nickel sulfides were investigated with XRD. As depicted
152 in **Fig. 2d**, most of the strong peaks in the XRD patterns of NiS-NW/NF and NiS-NP/NF are
153 matched to Ni_3S_2 (JCPDS No. 71-1682) and NiS (JCPDS No. 86-2280), indicating that the two
154 nickel sulfide samples are mainly composed of Ni_3S_2 and NiS. The diffraction peaks at 21.7º,
155 31.0º, 37.7º, 38.2º, 44.3º, 49.6º, 50.0º, and 55.2º can be assigned to (1 0 1), (1 1 0), (0 0 3), (0 2 1),
156 (2 0 2), (1 1 3), (2 1 1), and (1 2 2) reflection planes of Ni_3S_2, respectively; whereas those at 18.3º,
157 30.2º, 32.1º, 35.7º, 40.4º, 48.8º, 50.1º, 52.6º, and 57.3º can be indexed to (1 -1 0), (1 0 1), (3 0 0),
158 (0 2 1), (2 1 1), (1 3 1), (4 1 0), (4 0 1), and (3 3 0) reflection planes of NiS, respectively. Apart
159 from Ni_3S_2 and NiS, the strong peaks of metallic Ni are still observed on the patterns of nickel
160 sulfide samples, suggesting that the nickel foam is partially sulfurized. Further insights into the

nanostructure of NiS NWs are provided by the TEM analysis. **Fig. 2e** presents a typical high magnification TEM image of NiS NWs, the crystal lattices of NiS NWs can be indexed to Ni_3S_2 and NiS with a clear interface. The lattice distances of 0.28 and 0.48 nm correspond to the (1 1 0) and (1 -1 0) crystal planes of Ni_3S_2 and NiS, respectively. The results from the TEM image are line with the XRD analysis.

X-ray photoelectron spectroscopic (XPS) analysis was employed to ascertain the elemental composition and the electronic structure of the NiS-NW/NF sample. The survey spectrum suggests the presence of Ni and S elements in the sample (**Fig. S1**). As depicted in **Fig. 3a**, the appreciable peaks at 854.7 and 872.1 eV are attributed to the Ni^{2+} state, and the distinct peaks at 856.1 and 873.7 eV are correspond to the Ni^{3+} state. These results suggest the co-existence of NiS and Ni_3S_2 in NiS-NW/NF [29]. Meanwhile, the high-resolution spectrum of S 2p in **Fig. 3b** displays three fitting peaks at 169.1 eV, 163.8 eV and 162.6 eV, which can be assigned to SO_4^{2-}, S $2p_{1/2}$ and S $2p_{3/2}$ in NiS-NW/NF, respectively, and the presence of SO_4^{2-} is mainly due to surface oxidation.

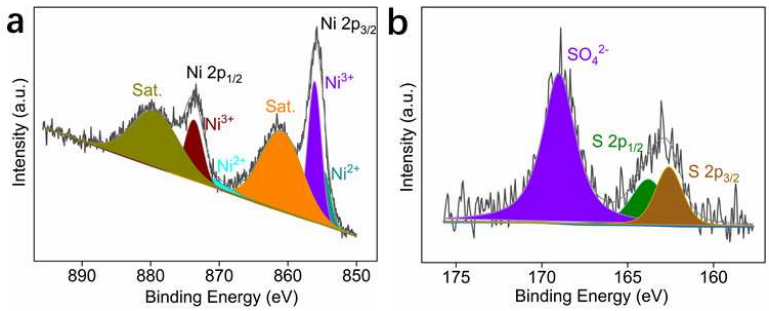

Figure 3. XPS spectra of NiS-NW/NF. (a) the Ni 2p spectrum and (b) the S 2p spectrum.

3.2. Electrocatalytic performance

The oxygen evolution activity of the as-prepared nickel sulfide samples was examined in the

oxygen-saturated 1.0 M KOH solution. For comparison, the OER performances of acid treated bare NF and IrO_2/NF were also tested under the same experimental conditions. As shown in **Fig. 4a**, NiS-NW/NF requires a substantial lower overpotential of 279 mV to obtain 100 mA cm^{-2} compared to NiS-NP/NF (300 mV), and IrO_2/NF (315 mV). The peaks ranging from 1.3 to 1.4 V vs. RHE for the LSV curves of are ascribed to the oxidation of Ni^{2+} to Ni^{3+}. Furthermore, at the anodic current densities of 200 mA cm^{-2} and 400 mA cm^{-2}, the applied overpotential of NiS-NW/NF are 334 mV and 398 mV respectively, significantly lower than those of NiS-NP/NF (450 mV and 652 mV) (**Fig. 4b**). **Fig. 4c** shows that NiS-NW/NF delivers a lower Tafel slope (38.44 mV dce^{-1}) than NiS-NP/NF (88.03 mV dce^{-1}) and NF (89.51 mV dce^{-1}), suggesting the OER kinetics of NiS-NW/NF is superior to the that of NiS-NP/NF and NF. These results of overpotentials and Tafel slopes reveal that NiS-NW/NF indeed exhibits efficient OER performances (η_{100} = 279 mV, Tafel slope = 38.44 mV dce^{-1}), which are much better than NiS-NP/NF (η_{100} = 300 mV, Tafel slope = 88.03 mV dce^{-1}). In addition, the OER activities ($\eta_{100,}$ Tafel slope) of NiS-NW/NF outperform most of recently documented nickel sulfide-based OER catalysts (**Fig. 4d**) [29-41], such as NiCoS/NF (370 mV, 145 mV dce^{-1}) [36], Ni_3N-Ni_3S_2 (404 mV, 112 mV dce^{-1}) [37], CoS_x/Ni_3S_2@NF (373 mV, 105 mV dce^{-1}) [38], P-doped Ni_3S_2/NF (306 mV, 99 mV dce^{-1}) [39], Ni_3S_4 (340 mV, 67 mV dce^{-1}) [41].

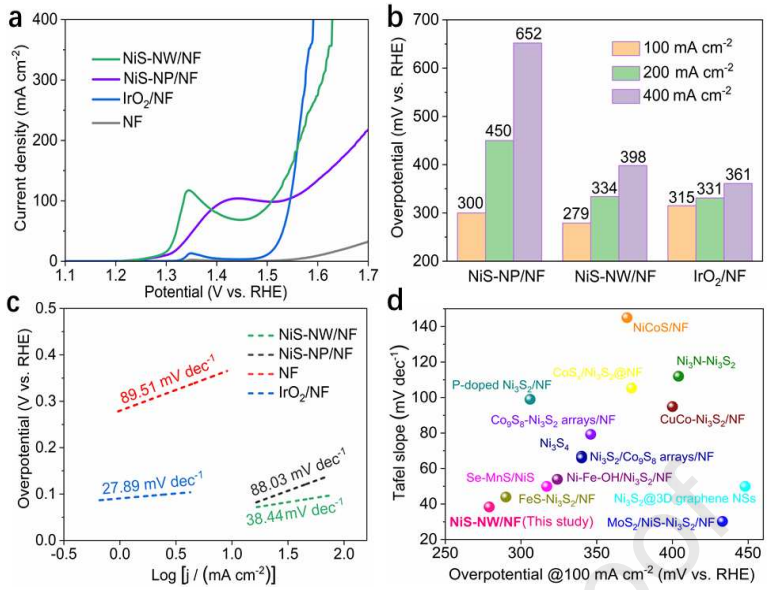

Fig. 4 (a) LSV curves of the OER performance of Ni foam, NiS-NW/NF, NiS-NP/NF, and IrO_2/NF in 1.0 M KOH at a scan rate of 5 mV s^{-1}. (b) Comparison of overpotentials at 100, 200, and 400 mA cm^{-2} of NiS-NW/NF, NiS-NP/NF, and IrO_2/NF. (c) Tafel plots of Ni foam, NiS-NW/NF, NiS-NP/NF, and IrO_2/NF. (d) Comparison of overpotential and Tafel slope of OER between the NiS-NW/NF and reported nickel sulfide-based catalysts.

To probe the charge-transfer kinetics and the ECSA of catalysts, C_{dl} and EIS were measured. C_{dl} is a convincing parameter for the estimation of accessible active sites of electrocatalysts, as the C_{dl} is positively proportional to ECSA (ECSA = C_{dl}/C_s, where C_s is the specific capacitance). The C_{dl} was measured via CV scans in the non-faradic potential region (1.1 - 1.2 V vs. RHE) at various scan rates (40, 60, 80, 100, 120 mV/s) (**Fig. 5a-c**). The capacitive current density differences (△ j= (j_a-j_c)/2) at 1.15 V vs. RHE as a function of scan rate displays the C_{dl} values of catalysts (**Fig. 5d**). The calculated C_{dl} values of NiS-NW/NF, NiS-NP/NF and NF are 39.42, 10.36, and 2.88 mF cm^{-2}, respectively. The high C_{dl} value means NiS-NW/NF possesses a much higher ECSA in

comparison to that of NiS-NP/NF and NF, suggesting that NiS-NW/NF exposes more electroactive sites for the electrocatalytic water oxidation reaction. To further investigate the OER kinetics, EIS was also measured. **Fig. 5e** presents the Nyquist plots of NiS-NW/NF, NiS-NP/NF and NF. The Nyquist plot of NiS-NW/NF shows a smaller semicircle than that of NiS-NP/NF and NF in the high frequency region. The fitting results suggest that NiS-NW/NF exhibits a smaller charge transfer resistance (R_{ct}) (4.84 Ω) than that of NiS-NP/NF (21.11 Ω) and NF (67.11 Ω), revealing faster charge transfer and the smaller charge transfer resistance of the NiS-NW/NF during the OER process.

In this study, the chronoamperometry (CA) measurement was conducted at a constant potential of 1.5 V vs. RHE to evaluate the durability of NiS-NW/NF toward OER. As depicted in **Fig. 5f**, the current density remains stable after 12 h running, and only about 5% current density loss happened on the NiS-NW/NF electrode. This result indicates that the NiS-NW/NF exhibits good stability under alkaline conditions. In addition, the XPS test was performed to examine the chemical state of the pre-catalytic and post-OER NiS-NW/NF. There is no obvious change observed for signals for the Ni species (**Fig. S2**) for the catalyst after the OER electrocatalysis. However, the S 2p spectra show that the intensity of S peaks decreases significantly after the long-term OER test (**Fig. S3**), indicating the surface oxidation of NiS-NW/NF.

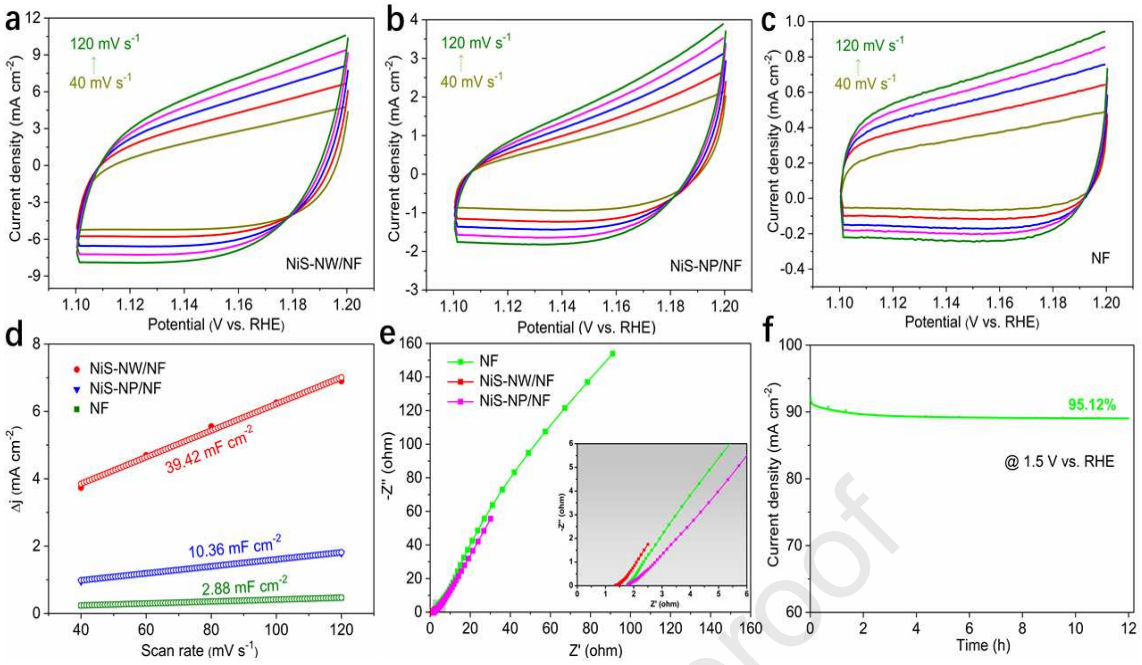

Fig. 5 (a-c) Cyclic voltammograms of NiS-NW/NF, NiS-NW/NF, and nickel foam at different scan rates (from 40 to 120 mV s^{-1} with an increment of 20mV s^{-1}). (d) Scan rate dependence of the current densities of NiS-NW/NF, NiS-NW/NF, and nickel foam at 1.15 V vs. RHE, (e) Nyquist plots at the open circuit potential, (f) Amperometric i-t curve of NiS-NW/NF at an applied potential of 1.5 V versus RHE.

Moreover, the HER activity of NiS-NW/NF, NiS-NP/NF and NF was also measured in N_2-saturated 1.0 M KOH. The overpotentials required to reach 20 mA cm^{-2} are determined to be 224, 228, and 415 mV vs. RHE for NiS-NW/NF, NiS-NP/NF and NF, respectively (**Fig. 6a**). This comparison clearly shows that NiS-NW/NF exhibits a lower overpotential than NiS-NP/NF. However, the HER performances of NiS catalysts in this study are inferior to those of the 20 wt % Pt/C benchmark catalyst which only takes 92.6 mV to achieve a current density of 20 mA cm^{-2}. Although the 20 wt % Pt/C catalyst exhibits the smallest Tafel slope (72.35 mV dec^{-1}), the Tafel slope of NiS-NW/NF (116.24 mV dec^{-1}) is lower than that of NiS-NP/NF (122.37 mV dec^{-1}) and

NF (163.94 mV dec^{-1}) (**Fig. 6b**). These results suggest that NiS-NW/NF exhibits improved HER activity compared to NiS-NP/NF, demonstrating the advantage of the dimensionally constructed heterogeneous nanoworm structure with multi-level interfaces. Moreover, the excellent HER performance of NiS-NW/NF is also attributed to abundant exposure of electroactive sites owing to the high surface area. Apart from the favorable HER activity, NiS-NW/NF also shows good durability in 1 M KOH. The results displayed in **Fig. S4** suggest the electrocatalytic activity of hydrogen evolution decreases very little after 12 h electrocatalysis.

As the synthesized catalyst showcases good electrocatalytic activities toward both OER and HER in the alkaline solution, a two-electrode single cell system was constructed using NiS-NW/NF as both cathode and anode to investigate its overall water splitting competency. For comparison, the performance of NiS-NP/NF was also tested. Impressively, the current density of 10 mA cm^{-2} is achieved obtained at a low cell voltage of 1.563 V over the NiS-NW/NF||NiS-NW/NF, which is smaller than that of 1.643 V over the NiS-NP/NF||NiS-NP/NF (**Fig. 6c**). At a constant potential of 1.563 V, NiS-NW/NF shows a negligible change of current density after continuous operation for 12 h (**Fig. 6d**), which indicates its great durability. As a catalyst for overall water splitting, the NiS-NW/NF shows favorable catalytic activity and structural stability, directing an efficient and large-scale synthetic strategy for binder-free catalysts in renewable energy conversion.

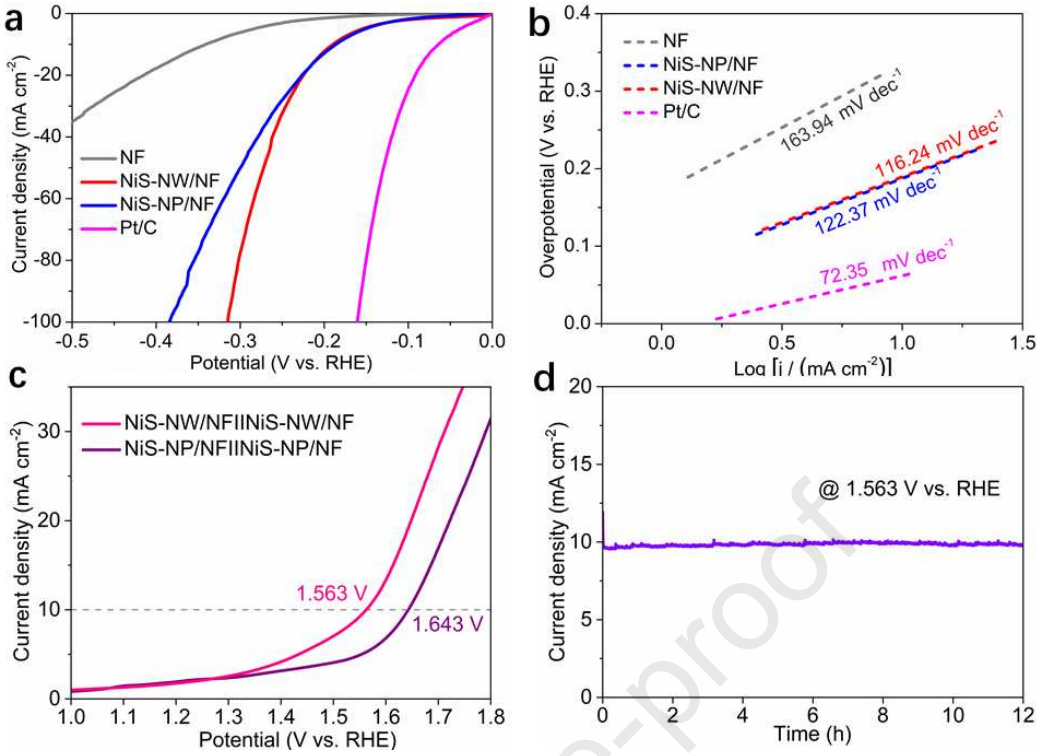

Fig. 6 (a) LSV curves of the HER performance of NiS-NW/NF, NiS-NW/NF, nickel foam, and 20 wt % Pt/C, (b) corresponding Tafel plots, (c) LSV curve of water electrolysis using NiS-NW/NF or NiS-NW/NF as both HER and OER electrocatalysts in a two-electrode configuration, (d) Amperometric i-t curve of NiS-NW/NF for water splitting at an applied potential of 1.563 V.

4. Conclusions

In summary, we have synthesized a nanoworm-like nickel sulfide nanostructure via a one-step solvothermal method. With a smaller size, larger electrochemical surface area, and lower charge transfer resistance, the as-prepared nanoworm-like nickel sulfides (NiS-NW/NF) perform better than the nanoplate-like counterpart. The NiS-NW/NF only takes a low overpotential of 279 mV to obtain 100 mA cm^{-2} for OER, exceeding most of reported nickel sulfide-based catalysts. In addition, when used as a bifunctional catalyst for overall water splitting, the NiS-NW/NF achieves a current density of 10 mA cm^{-2} at only 1.563 V with good long-term durability. This study

provides a facile and effective strategy for the design and development of cost-effective catalysts for water splitting.

CRediT authorship contribution statement

Zhijie Chen: Experiments, Conceptualization, Discussions, Writing. **Idris Ibrahim**: Material synthesis, Discussions. **Derek Hao**: Writing, Data analysis, Discussions. **Xiaoqing Liu**: Data analysis, Discussions. **Lan Wu**: Data analysis, Discussions. **Wei Wei**: Data analysis, Discussions. **Dawei Su**: Data analysis, Discussions. **Bing-Jie Ni**: Discussions, Writing, Project acquisition.

Declaration of Competing Interest

The authors declare no competing financial interest.

Acknowledgements

This work is supported by the Australian Research Council (ARC) Future Fellowship (FT160100195). Mr. Zhijie Chen acknowledges the China Scholarship Council (CSC) for the scholarship support.

References

[1] H. Wan, X. Liu, H. Wang, R. Ma, T. Sasaki, Recent advances in developing high-performance nanostructured electrocatalysts based on 3d transition metal elements, Nanoscale Horiz. 4 (2019) 789-808.

[2] Z. Chen, X. Duan, W. Wei, S. Wang, B.-J. Ni, Recent advances in transition metal-based electrocatalysts for alkaline hydrogen evolution, J. Mater. Chem. A 7 (2019) 14971-15005.

[3] B. You, Y. Sun, Innovative strategies for electrocatalytic water splitting, Acc. Chem. Res. 51 (2018) 1571-1580.

[4] Q. Shi, S. Fu, C. Zhu, J. Song, D. Du, Y. Lin, Metal-organic frameworks-based catalysts for electrochemical oxygen evolution, Materials Horiz. 6 (2019) 684-702.

[5] Z. Chen, X. Duan, W. Wei, S. Wang, Z. Zhang, B.-J. Ni, Boride-based electrocatalysts: Emerging candidates for water splitting, Nano Res. 13 (2020) 293-314.

[6] Z. Chen, W. Wei, B.-J. Ni, Cost-effective catalysts for renewable hydrogen production via electrochemical water splitting: Recent advances, Curr. Opin. Green Sustain. Chem. 27 (2021) 100398.
[7] L. Lv, Z. Yang, K. Chen, C. Wang, Y. Xiong, 2D layered double hydroxides for oxygen evolution reaction: From fundamental design to application, Adv. Energy Mater. 9 (2019) 1803358.
[8] P. Yu, F. Wang, T.A. Shifa, X. Zhan, X. Lou, F. Xia, J. He, Earth abundant materials beyond transition metal dichalcogenides: A focus on electrocatalyzing hydrogen evolution reaction, Nano Energy 58 (2019) 244-276.
[9] J. Li, G. Zheng, One-dimensional earth-abundant nanomaterials for water-splitting electrocatalysts, Adv. Sci. 4 (2017) 1600380.
[10] M.Q. Yang, J. Wang, H. Wu, G.W. Ho, Noble metal-free nanocatalysts with vacancies for electrochemical water splitting, Small 14 (2018) e1703323.
[11] B. Zhu, R. Zou, Q. Xu, Metal-organic framework based catalysts for hydrogen evolution, Adv. Energy Mater. 8 (2018) 1801193.
[12] S. Zhao, Y. Wang, J. Dong, C.-T. He, H. Yin, P. An, K. Zhao, X. Zhang, C. Gao, L. Zhang, Ultrathin metal-organic framework nanosheets for electrocatalytic oxygen evolution, Nat. Energy 1 (2016) 1-10.
[13] X. Liu, L. Dai, Carbon-based metal-free catalysts, Nat. Rev. Mater. 1 (2016) 16064.
[14] C. Hu, L. Dai, Doping of carbon materials for metal-free electrocatalysis, Adv. Mater. 31 (2019) e1804672.
[15] D. Liu, L. Dai, X. Lin, J.F. Chen, J. Zhang, X. Feng, K. Mullen, X. Zhu, S. Dai, Chemical approaches to carbon-based metal-free catalysts, Adv. Mater. 31 (2019) e1804863.
[16] S. Zhao, D.W. Wang, R. Amal, L. Dai, Carbon-based metal-free catalysts for key reactions involved in energy conversion and storage, Adv. Mater. 31 (2019) 1801526.
[17] S. Zhao, X. Lu, L. Wang, J. Gale, R. Amal, Carbon-based metal-free catalysts for electrocatalytic reduction of nitrogen for synthesis of ammonia at ambient conditions, Adv. Mater. 31 (2019) 1805367.
[18] Y. Guo, T. Park, J.W. Yi, J. Henzie, J. Kim, Z. Wang, B. Jiang, Y. Bando, Y. Sugahara, J. Tang, Y. Yamauchi, Nanoarchitectonics for transition□metal□sulfide□based electrocatalysts for water splitting, Adv. Mater. 31 (2019) 1807134.
[19] J. Hou, Y. Wu, B. Zhang, S. Cao, Z. Li, L. Sun, Rational design of nanoarray architectures for electrocatalytic water splitting, Adv. Funct. Mater. 29 (2019) 1808367.
[20] J. Joo, T. Kim, J. Lee, S.I. Choi, K. Lee, Morphology-controlled metal sulfides and phosphides for electrochemical water splitting, Adv. Mater. 31 (2019) e1806682.
[21] T. Sun, G. Zhang, D. Xu, X. Lian, H. Li, W. Chen, C. Su, Defect chemistry in 2D materials for electrocatalysis, Mater. Today Energy 12 (2019) 215-238.
[22] Y. Zhang, L. Guo, L. Tao, Y. Lu, S. Wang, Defect-based single-atom electrocatalysts, Small Methods 3 (2018) 1800406.
[23] T. Tang, W.-J. Jiang, S. Niu, L.-P. Yuan, J.-S. Hu, L.-J. Wan, Hetero-coupling of a carbonate hydroxide and sulfide for efficient and robust water oxidation, J. Mater. Chem. A 7 (2019) 21959-21965.
[24] T.A. Shifa, F. Wang, Y. Liu, J. He, Heterostructures based on 2D materials: A versatile platform for efficient catalysis, Adv. Mater. 31 (2018) e1804828.
[25] Z. Chen, X. Duan, W. Wei, S. Wang, B.-J. Ni, Iridium-based nanomaterials for electrochemical water splitting, Nano Energy 78 (2020) 105270.
[26] X. Wu, X. Han, X. Ma, W. Zhang, Y. Deng, C. Zhong, W. Hu, Morphology-controllable synthesis

of Zn-Co-mixed sulfide nanostructures on carbon fiber paper toward efficient rechargeable zinc–air batteries and water electrolysis, ACS Appl. Mater. Interfaces 9 (2017) 12574-12583.

[27] B. You, N. Jiang, Y.J. Sun, Morphology-activity correlation in hydrogen evolution catalyzed by cobalt sulfides, Inorg. Chem. Front. 3 (2016) 279-285.

[28] Z. Chen, Y. Liu, W. Wei, B.-J. Ni, Recent advances in electrocatalysts for halogenated organic pollutant degradation, Environ. Sci.: Nano 6 (2019) 2332-2366.

[29] Y. Guan, H. Xuan, H. Li, P. Han, Synthesis of 3D flower-like nickel-molybdenum-sulfur microspheres as efficient and stable electrocatalyst for hydrogen and oxygen evolution reactions, Electrochim. Acta 320 (2019) 134614.

[30] F. Wu, X. Guo, G. Hao, Y. Hu, W. Jiang, Synthesis of iron-nickel sulfide porous nanosheets via a chemical etching/anion exchange method for efficient oxygen evolution reaction in alkaline media, Adv. Mater. Interfaces 6 (2019) 1900788.

[31] B. Li, Z. Li, F. He, Q. Pang, P. Shen, One-pot preparation of Ni_3S_2@3-D graphene free-standing electrode by simple Q-CVD method for efficient oxygen evolution reaction, Int. J. Hydrogen Energy 44 (2019) 30806-30819.

[32] W. He, G. Ren, Y. Li, D. Jia, S. Li, J. Cheng, C. Liu, Q. Hao, J. Zhang, H. Liu, Amorphous nickel-iron hydroxide films on nickel sulfide nanoparticles for the oxygen evolution reaction, Catal. Sci. Technol. 10 (2020) 1708-1713.

[33] J. Zhu, M. Sun, S. Liu, X. Liu, K. Hu, L. Wang, Study of active sites on Se-MnS/NiS heterojunctions as highly efficient bifunctional electrocatalysts for overall water splitting, J. Mater. Chem. A 7 (2019) 26975-26983.

[34] J. Lin, H. Wang, X. Zheng, Y. Du, C. Zhao, J. Qi, J. Cao, W. Fei, J. Feng, Controllable synthesis of core-branch Ni_3S_2/Co_9S_8 directly on nickel foam as an efficient bifunctional electrocatalyst for overall water splitting, J. Power Sources 401 (2018) 329-335.

[35] J.-F. Qin, M. Yang, S. Hou, B. Dong, T.-S. Chen, X. Ma, J.-Y. Xie, Y.-N. Zhou, J. Nan, Y.-M. Chai, Copper and cobalt co-doped Ni_3S_2 grown on nickel foam for highly efficient oxygen evolution reaction, Appl. Surf. Sci. 502 (2020) 144172.

[36] K.-L. Yan, X. Shang, Z. Li, B. Dong, J.-Q. Chi, Y.-R. Liu, W.-K. Gao, Y.-M. Chai, C.-G. Liu, Facile synthesis of binary NiCoS nanorods supported on nickel foam as efficient electrocatalysts for oxygen evolution reaction, Int. J. Hydrogen Energy 42 (2017) 17129-17135.

[37] Y. Zhao, B. Jin, A. Vasileff, Y. Jiao, S.-Z. Qiao, Interfacial nickel nitride/sulfide as a bifunctional electrode for highly efficient overall water/seawater electrolysis, J. Mater. Chem. A 7 (2019) 8117-8121.

[38] S. Shit, S. Chhetri, W. Jang, N.C. Murmu, H. Koo, P. Samanta, T. Kuila, Cobalt sulfide/nickel sulfide heterostructure directly grown on nickel foam: An efficient and durable electrocatalyst for overall water splitting application, ACS Appl. Mater. Interfaces 10 (2018) 27712-27722.

[39] Y. Ding, H. Li, Y. Hou, Phosphorus-doped nickel sulfides/nickel foam as electrode materials for electrocatalytic water splitting, Int. J. Hydrogen Energy 43 (2018) 19002-19009.

[40] Y. Zhou, S. Xi, X. Yang, H. Wu, In situ hydrothermal growth of metallic Co_9S_8-Ni_3S_2 nanoarrays on nickel foam as bifunctional electrocatalysts for hydrogen and oxygen evolution reactions, J. Solid State Chem. 270 (2019) 398-406.

[41] K. Wan, J. Luo, C. Zhou, T. Zhang, J. Arbiol, X. Lu, B.W. Mao, X. Zhang, J. Fransaer, Hierarchical porous Ni_3S_4 with enriched high-valence Ni sites as a robust electrocatalyst for efficient oxygen evolution reaction, Adv. Funct. Mater. 29 (2019) 1900315.

Highlights

1. The nanoworm-like nickel sulfides (NiS) were designed by a facile solvothermal process
2. The solvothermal precursors govern the nanostructure of NiS
3. The nanoworm-like NiS outperform the nanoplate-like counterpart for water splitting
4. The nanoworm-like NiS exhibit good activity and stability for overall water splitting

Declaration of interests

☒ The authors declare that they have no known competing financial interests or personal relationships that could have appeared to influence the work reported in this paper.

☐The authors declare the following financial interests/personal relationships which may be considered as potential competing interests: